Interactions between Surfaces Bearing Highly Extended Polymer Melt Brushes. 1. Adhesion and Spontaneous Thinning

Larisa Tsarkova,[†,⊥] Xueyan Zhang,[†,#] Jacob Klein,[*,†,‡] and Nikos Hadjichristidis[§]

Weizmann Institute of Science, Rehovot, 76100, Israel; Physical and Theoretical Chemistry Laboratory, Oxford University, Oxford 0X1 3QZ, U.K.; and Department of Chemistry, University of Athens, Panepistimiopolis, Zografou, 157 71 Athens, Greece

Received June 6, 2001; Revised Manuscript Received December 11, 2001

ABSTRACT: A surface force balance (SFB) was used to characterize the behavior of highly stretched polymer brush melts. Langmuir−Blodgett monolayers of polyisoprene (M_w = 29.9 kg/mol) end-functionalized with a zwitterionic group were deposited onto freshly cleaved mica (areal density ≈ 1 chain/(170 Å^2)), and two identical brush monolayers were brought into adhesive contact in the SFB. The changes in film thickness as well as the topography of the contact could be continuously monitored. We observed spontaneous film thinning of the brush-melt bilayer, attributed to the outward lateral motion of the anchoring end groups resulting from the contact-induced pressure on the confined brushes, and a detailed model for this is presented. Refractive index measurements of the confined PI-X melt brushes did not reveal any significant deviation from the bulk value for polyisoprenes, suggesting that possible effects (if any) on the optical properties due to chain orientation were below our detection limit. The behavior of the two opposing brush melts was compared with that where only one brush monolayer was confined between mica surfaces.

Introduction

Polymer chains that are densely end-attached to solid surfaces form an extended brushlike structure that can strongly modify surface behavior. Such brushes in a good solvent have served as a paradigm for theoretical and experimental studies of surface modification.[1−9] In addition, they are used to control material properties ranging from colloidal stability[10,11] to wettability[12] and lubrication.[13,14] The clear practical and fundamental interest in such brushes has led to their being intensively studied, using a large variety of approaches. The case of interactions between densely attached, solvent-free polymer *melt* brushes provides an extreme limit which is of considerable interest but which has been relatively neglected in comparison. A number of models discussing the interpenetration of two compressed polymer melt brushes, as well as their shear and relaxation properties when they slide laterally past each other, have been presented,[15−17] but to our knowledge there have been no experimental studies to date of shear interactions between polymer brush melts. A number of studies have examined the shear forces between surfaces across highly confined polymer melts,[18−20] where the chains are not end-attached to the substrates, and these have been interpreted largely in terms of thin-film polymer melt rheology. The advantage of working with polymer melt brushes is that the structure and surface density of the chains are well characterized, a single, densely end-attached monolayer being associated with each interacting solid surface. This in turn enables an unambiguous surface molecular interpretation of both the equilibrium and dynamic features of the interactions.

The purpose of the present study is to create surface layers of polymer melt brushes on solid substrates and to examine their normal and shear interactions using a surface force balance (SFB). The usual way of attaching polymer brushes onto surfaces is via self-assembly of end-functionalized chains[6] or diblock copolymers[4] from solution, ensuring that only one end of the chain attaches and that the dangling tail does not adsorb to the substrates. Extending this approach to create a melt brush is in principle possible, by washing away free polymer and then thoroughly drying the solvent, and indeed has been done.[21,22] However, typical surface densities achievable by this approach clearly mimic those achieved by self-assembly from solution and are limited by the balance between osmotic repulsion and end-attachment energy. The values that may be achieved in this way are thus relatively low and result in rather thin layers when in the dry (melt) state—typically only 1 nm thick,[21,22] much less than the chains' radius of gyration—thereby losing the defining feature which distinguishes brush structure and properties. An alternative and interesting approach to create high surface densities of end-attached chains is by polymerization from a dense array of surface initiation sites. This has been utilized recently[23] to create dense, though rather polydispersed, end-attached polymer layers in a good solvent.

Recently, Heger and Goedel[24] investigated the properties of insoluble monolayers of polyisoprenes on a water surface, where each polymer chain was end-functionalized with a sulfonate group. They assumed that each polymer chain was bound to the water phase via its end group and had the conformation of a distorted three-dimensional coil. The experimentally observed linear increase of lateral surface pressure with the chain length for a given area per headgroup (measured with a Langmuir balance) was fitted using a thermodynamic

† Weizmann Institute of Science.
‡ Oxford University.
§ University of Athens.
⊥ Present address: Department of Chemistry, Moscow State University, Moscow 119899, Russia.
Present address: Newark College Of Engineering, New Jersey Institute of Technology, University Heights, Newark, NJ 07102.
* Corresponding author. E-mail jacob.klein@chem.ox.ac.uk or jacob.klein@weizmann.ac.il.

10.1021/ma010981f CCC: $22.00
Published on Web 02/21/2002

description of confined brushes with different molecular weights. When transformed to solid substrates, these monolayers create dense incompressible brush melts with controllable grafting density and thickness.

The present work measures the interactions between well-characterized, highly stretched molten brush layers created in this manner. In this paper (paper 1) we focus on the issue of the normal (adhesive) interaction of two opposing brushes. The shear behavior of the same systems will be reported in paper 2.[25] We first discuss the properties of the brush melt, which follow directly from the preparation procedure, and the brush−brush interactions, particularly the thinning of the brush bilayer following adhesive contact between the surfaces. Further we examine the behavior of a single brush monolayer interacting with a bare solid surface. Finally, we present a detailed model for the thinning of the brush bilayers from between the underlying solid substrates which may be compared with our experimental thinning results.

Experimental Section

Materials. *Polymers.* Linear polyisoprene (PI) end-terminated by the zwitterionic group $-(CH_3)_2N^+(CH_2)_3SO_3^-$ (designated -X) has been used to obtain stretched brush monolayers (its structure is the inset in Figure 3). We refer to these end-functionalized chains as PI-X. They were synthesized as follows: Isoprene was polymerized in an evacuated, *n*-BuLi washed and solvent rinsed glass reactor, at room temperature in a 9:1 mixture of cyclohexane and benzene. The polymerization was initiated by 3-(dimethylamino)propyllithium, resulting in a tertiary amine group on each polyisoprene chain. The living ends were terminated, under vacuum, by a small amount of degassed methanol, and the dimethylamine-capped polyisoprene (PI-NMe_2) was isolated by precipitation in methanol containing 0.02% of 2,6-di-*tert*-butyl-*p*-cresol as antioxidant. The tertiary amine groups were converted to sulfozwitterions by reaction with cyclopropane sultone:

$$PI{-}NMe_2 + O{=}S(O(CH_2)_3){=}O \rightarrow PI{-}N^+Me_2(CH_2)_3SO_3^-$$

More details on the synthesis of PI-X are given elsewhere.[26] Structural and molecular characterization was carried out on the precursor amine-capped PI in order to avoid complications coming from the self-association of the strong sulfozwitterionic dipoles. The parameters of the zwitterion-terminated PI-X should be the same. The microstructure was found (^{13}C NMR, $CHCl_3$, 30 °C) to be the following: 55 wt % 1,4-cis; 29 wt % 1,4-trans; and 16 wt % 3,4. The 3,4-content, which is higher than that of PI obtained with *sec*-BuLi, is consistent with the known modifying effect of tertiary amines on polydienes microstructure.[27] The molecular characteristics of the amine-capped PI are given below: $M_n = 28\,300$ (membrane osmometry, toluene at 30 °C, Wescan 231); $M_w = 29\,900$ (low-angle laser light scattering, THF at 25 °C, $\lambda = 633$ nm, Chromatix KMX-6, $dn/dc = 0.128$ mL/g under the same conditions, Chromatix KMX-16). $M_w/M_n = 1.06$ (size exclusion chromatography, THF at 30 °C, Waters).

The polymer is an amorphous, viscous liquid at room temperature, with a glass transition temperature $T_g = -66$ °C.[28] The glass transition temperature was reported to be unchanged by the sultone reaction.[29] Other relevant parameters are as follows: unperturbed end-to-end dimension[30] $R_0 = (0.8M_w^{1/2}) = 137$ Å; viscosity $\eta_0 = 9.38 \times 10^{-15}M_w^{3.66} = 230$ Pa·s at the temperature of our experiments (25 °C), and entanglement weight $M_w = 5300$ for polyisoprene.[31] The surface tension of pure polyisoprene has been reported as 31 mN/m, and the density of the polymer $\rho = 0.913$ g/cm^3.[32]

Dried samples of PI-X were stored in a deep freezer until used. Direct contact with alcohols and water was avoided to minimize opportunities to hydrogen-bond complexation by the zwitterions.

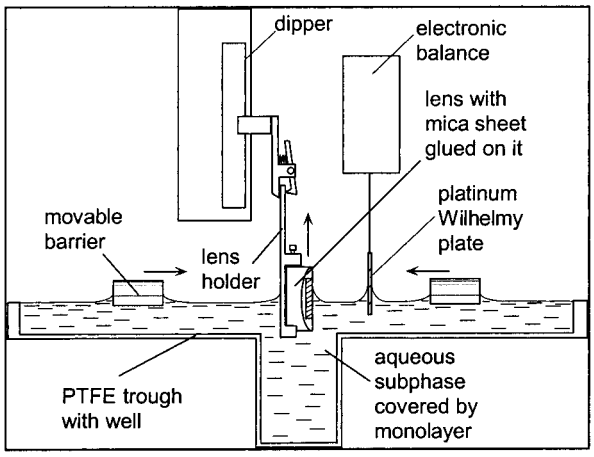

Figure 1. Schematic of the Langmuir−Blodgett deposition device used in the present experiments. The monolayers of PI-X were prepared using a 36 cm × 15 cm rectangular LB minitrough (KSV, Finland) made of poly(tetrafluoroethylene), equipped with two compression hydrophilic barriers and a Wilhelmy platinum plate for the detection of the surface pressure. All depositions were carried out by withdrawing the substrates from the water subphase at a constant pressure of 15 mN/m. Mica sheets glued to cylindrical glass lenses previously calibrated in the SFB (see Figure 2) were used as substrates. Deposition on both lenses was carried out simultaneously at speed 2 mm/min, following which the lenses were remounted in the SFB.

Apparatus and Experimental Procedure. *Langmuir−Blodgett (LB) Preparation and Deposition.* The monolayers of PI-X for SFB studies were prepared using a 36 cm × 15 cm rectangular Langmuir−Blodgett minitrough made of poly(tetrafluoroethylene), equipped with two compression hydrophilic barriers and Wilhelmy Pt plate for the detection of the surface pressure and dipper device (KSV, Finland). The water used (resistivity 18.2×10^6 Ω/cm, total dissolved organic carbon < 4 ppm) was purified by a Millipore system (activated charcoal treated tap water passed through a reverse osmosis (RiOs) stage and finally by a Milli-Q Gradient A10 ion-exchange unit).

Polymers were spread on the surface of pure water from 0.01 wt % solutions in hexane (Merck, spectroscopic grade), and the layer was compressed to a predetermined pressure. Prior to deposition, the stability of the layer was checked over a 10−15 min period. All depositions were carried out by withdrawing the substrates from the water subphase at constant pressure 15 mN/m. Freshly cleaved mica sheets (Ruby Clear Muscovite mica, Grade 1, purchased from S & J Trading Inc., New York) glued to glass lens supports (EPON 1004 epoxy glue) were used throughout as substrates. Deposition on both lenses was carried out simultaneously at 2 mm/min withdrawal speed. Figure 1 shows the LB setup schematically. The transfer ratio, determined in separate experiments with rectangular mica sheets, was close to 1. We note that upon withdrawing the lenses from the water subphase a residual interfacial layer of water may remain on mica, protected from rapid drying using conventional means (nitrogen flow or P_2O_5) by the thick polymer film.

Surface Forces Measurements. The surface force balance (SFB) used in the present study has recently been described in detail, in particular with respect to its high sensitivity and resolution in lateral motion and in measuring shear forces.[33] A schematic of the main elements is shown in Figure 2.

In this paper we focus on the normal forces $F(D)$ between the curved mica sheets mounted in crossed cylinder geometry (mean radius $R \approx 1$ cm), particularly the adhesion forces, measured by monitoring the bending of a normal-force spring S_2 (spring constant $K_2 = 150$ N/m) on which the lower mica surface is mounted (Figure 2). Relative normal motion of the surfaces was effected via a three-stage mechanism, with the most delicate stage utilizing a piezoelectric tube (PZT) which

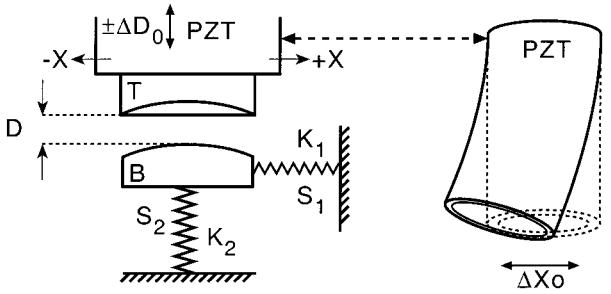

Figure 2. Schematic of the surface force balance (SFB) used in the present experiments (for details see ref 33). The two mica sheets are mounted on cylindrical quartz lenses in a crossed-cylinder configuration. The closest distance D between the surfaces is measured to ±2 Å using multiple-beam interferometry. The top lens is mounted on a sectored piezoelectric tube (PZT) which can move in the normal dorection ($\pm\Delta D_0$) or laterally ($\pm x$). Normal forces are measured via the bending of a horizontal leaf spring, shown schematically as the normal-force spring S_2 (spring constant K_2). Bending of the shear-force springs, shown schematically as S_1 (spring constant K_1), is monitored by capacitance changes of an air-gap capacitor to ±2 Å.

could apply both normal and lateral motion (here we consider normal motion ΔD only). The bending and the D values are determined using multiple beam interferometry with an accuracy of about ±3 Å, by monitoring the change in wavelength of fringes of equal chromatic order (FECO) in response to applied motion in the direction normal to the surfaces. As the surfaces come into adhesive contact once they touch, the radii of curvature are measured prior to contact and the area of flattened contact measured subsequently, to characterize the geometry of the interacting areas. In a number of cases images of the fringes have been taken using a video camera to illustrate the topography of the contact.

Adhesion and Interfacial Energy Measurements. Since the lower lens is suspended at the end of a cantilever spring, regions where the gradient of the force $dF(D)/dD$ is larger than the spring constant K_2 are inaccessible: at the distance where such intrinsic instabilities occur, the surfaces will jump to contact, driven by the attractive dispersion forces, or jump out when pulled apart. The value of the pull-off force, F_p, needed to separate the two surfaces from the contact, can be determined by multiplying the jump-out distance by the spring constant K_2. In our experiments the jump-out distances were of the order of tens of microns, which could not be determined from the position of the pth fringe. For this we used an approximate procedure:[34] on bringing the surfaces back into contact after jump out and counting the number q of fringes that have to pass the contact wavelength $\lambda_p°$ while approaching, one can readily evaluate the separation as $q\lambda_p°/2\mu$ (within a few percent accuracy), where μ is refractive index of the medium (air in our case).

The polyisoprene/air surface energy γ_{PI} may be determined according to the Johnson, Kendall, and Roberts (JKR) equation:[35]

$$\gamma_{PI} = -F_p/3\pi R \qquad (1)$$

where R is the radius of the curvature (ca. 1 cm) of the surfaces prior to contact. The radius of the flat contact area a_{exp} is measured directly from the fringe shape and was generally in the range 15−25 μm.

Refractive Index Measurements. The optical technique utilized in the SFB also allows the refractive index of the medium separating the mica surfaces to be determined. When the mica surfaces are brought to contact in the air, the positions $\lambda_p°$ and $\lambda_{p-1}°$ of two ECO fringes of pth and $(p-1)$th order are recorded, corresponding to the zero separation between the surfaces. If they are then separated by a distance D across a medium of uniform refractive index medium, a three-layer interferometer is formed. The fringes shift to longer wavelengths, with a different shift for odd and for even fringes. Measurements of wavelengths of two adjacent fringes (p, $p-1$) thus enable the evaluation not only of the distance between the surfaces but also of the refractive index of the medium separating them.[34]

Precise measurements of n require a precise simultaneous measurement of the position of the two adjacent ECO fringes. It was shown recently[36] that an error of only 0.5 Å in the measurement of the fringe wavelengths at contact (i.e., the calibration at zero separation) will prevent accumulation of reliable measurements, the effect being enhanced dramatically at short separations. In our experiments errors arose mainly from errors in determination of the contact position, as we have to dismount the mica-bearing lenses following initial calibration in order to deposit the film, and due to fringe drift during the thinning of the film (see Results). We note that due to birefringency of the mica, which results in interference fringes forming a doublet, measurements can be made based on either the left or right singlet of such a doublet.

The experimental procedure was as follows. In every experiment, the mica sheets were glued onto the cylindrical lenses, and the FECO wavelengths for air contact between the bare mica surfaces were calibrated in the SFB. Following this, the apparatus was opened in a dust-free laminar flow hood, the lenses were dismounted and fixed in the lens holders of the LB device (Figure 1), and the deposition of the PI-X was carried out. The lenses were then mounted back in the apparatus as close as possible to their original position. Before carrying out force measurements, the polymer layers were dried inside the box under dry nitrogen flow for several hours and experiments carried out under a dry nitrogen atmosphere. During an approach run the surfaces were moved slowly toward each other using the PZT, until they jumped into contact from a position roughly 50−100 Å from the polymer−polymer contact. No external compression load was applied following this jump into adhesive contact.

Results shown are from several different experiments, with data taken from a number of different contact positions in each experiment.

Results and Discussion

PI-X Monolayers at the Water/Air Interface. A typical isotherm of PI-X, shown in Figure 3, can be characterized as a $\pi-A$ isotherm of an expanded type, with collapse pressure above 37 mN/m. To obtain complete spreading, it is necessary to use highly diluted solutions of end-functionalized polymers—less than 0.01 wt %. This condition is dictated by the "critical association concentration" ($10^{-6}-10^{-7}$ M concentration of zwitterions), which was determined by light scattering measurements of diluted solutions of PI-X in aliphatic solvents.[29] The reasons for the poor spreading of PI-X from more concentrated solutions have been discussed by Heger and Goedel.[24] They suggested that in the bulk of the polymer phase polar end groups form clusters, which do not totally dissociate when dissolved in a hydrophobic solvent, and thus polar groups are sterically hindered from accessing the water surface. In this case the isotherm shifts to lower areas per headgroup. If dilution is observed, the monolayer is laterally homogeneous, and the isotherms are independent of the spreading conditions and compression speed and are nearly free of hysteresis.

We note that the isotherm we obtained for polyisoprene with a zwitterionic aminosulfonate end group is quite in line with the set of isotherms obtained earlier for polyisoprenes with different molecular weights and a polar sulfonate end group.[24] This suggests that we may relate to the thermodynamic properties of the similar hydrophobic polymer melt brushes developed in detail in the earlier study.

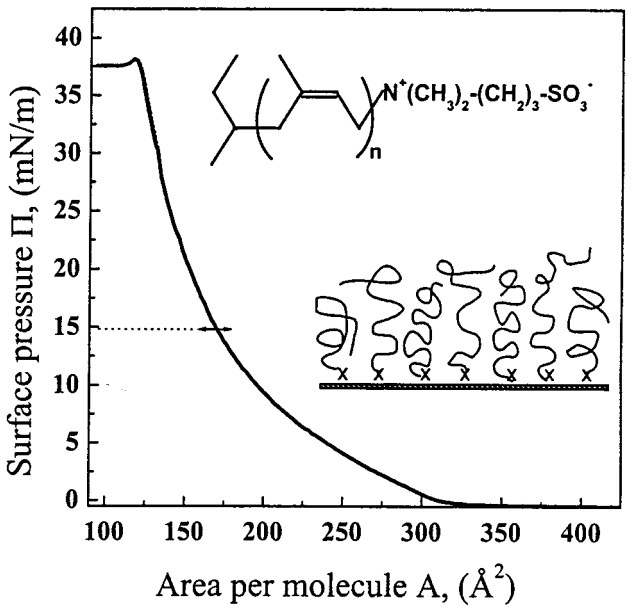

Figure 3. A typical isotherm of PI-X on the water subphase. The isotherm is of an expanded type, with collapse pressure above 37 mN/m. The dotted line is the deposition pressure. Upper inset: structure of the zwitterion-terminated polyisoprene (PI-X), where n is the degree of polymerization and -X is the group $-N^+(CH_3)_2-(CH_2)_3-SO_3^-$. Lower inset: illustrating the structure of the PI-X on the water subphase, with the zwitterionic group at the air−water interface.

Since the transfer ratio while depositing onto the solid substrate was close to 1, we may assume that the surface density of the monolayer is preserved, and we obtain on a freshly cleaved mica surface a well-defined highly stretched brush melt, composed of near monodisperse polymers with $N_w = 427$ monomers. The amount of polymer per unit area Γ and the thickness of the layer are determined from the parameters of the $\pi-A$ isotherm during deposition, that is, from the area per molecule $A = 170 \pm 6$ Å^2 at a surface pressure 15 mN/m. The thickness h of each monolayer is obtained directly as

$$h = (M/N_A)/\rho A \qquad (2)$$

where $M_n = 28\,300$ g/mol, $\rho = 0.913$ g/mL is the polymer density, and N_A is Avogadro's number. This gives for a monolayer thickness $h = 302 \pm 10$ Å. The contact separation following the jump in of the two mica surfaces each covered with PI-X monolayer, averaged from several experiments is 560 ± 20 Å. If we assume that this represents twice the thickness of an incompressible monolayer, this would correspond to each monolayer being on average 280 ± 10 Å, a height some 10% of the fully extended chain length. The two values of the monolayer thickness, obtained by completely different absolute approaches, are close to agreeing within their scatter. It may be that the small difference between them is due to thinning of the bilayer film (as described later) in the first few seconds after the surfaces jump into contact and before the initial determination of the contact position. Some contribution to the scatter in the thickness measured in the SFB may be due to the error introduced when remounting the surfaces in the appratus (following the brush deposition) in a slightly different relative orientation.

Other relevant parameters of the PI-X brush melt are the polymer adsorbance $\Gamma = 30$ mg/m^2, their surface number density (number of molecules per unit area) $= 1/A \approx 0.59 \times 10^{18}$ m^{-2}, and the mean distance between grafting ends, $s = \sqrt{A} \approx 13$ Å (compared to to the unperturbed end-to-end dimension $R_0 = 137$ Å and brush extension 280 Å). This ratio of brush height to interanchor spacing is very appreciably higher than in studies of solvated brushes to date.[1,4,6,7,37]

When deposited via the LB technique onto mica substrate, the PI-X monolayers have their polar zwitterionic headgroups—which were originally at the polymer−water interface—initially attached to the solid surface. From earlier studies[6] we know that the interaction energy $\epsilon_{zwitterion/mica}$ of the zwitterions with mica in a toluene medium is ca. $7-8\ k_BT$, and we may assume its value remains similar or even slightly higher when attached from a PI brush melt as in our experiments (because toluene is more polar than PI). The total energy associated with the PI chains in the brush stretched to an extent h is to a good approximation given by their stretching energy $E_{stretch}$, as there is no osmotic contribution in the conditions pertaining in the melt. This is given by[38] $E_{stretch} = (3h^2/2R_0^2)k_BT \approx 6k_BT$, comparable to or slightly lower than the zwitterion−mica sticking energy (ca. $8k_BT$). Moreover, the tension within each chain is of order $(\partial E_{stretch}/\partial h) \approx 0.05(k_BT/\text{Å})$. This compares with the much larger tension of order $(\epsilon_{zwitterion/mica}/2\ \text{Å}) \approx 4(k_BT/\text{Å})$ required to detach a zwitterion end group from the substrate, since pulling it away by say 2 Å from the mica surface presumably overcomes most of the sticking energy and so suffices to detach it. Thus, we would not expect the anchoring zwitterion ends within an uncompressed brush to be readily desorbed and removed from the surface due to the stretching, a process further inhibited kinetically by the high viscosity and entanglements within the PI-X brushes. This is indeed consistent with our observation that over the time scale of our experiments the initial film thickness and interactions (especially shear interactions[25]) of the unperturbed brushes remained generally the same from one contact position to another.

Opposing Brushes between Mica Surfaces. *Film Thinning.* One of the striking observations we made was that once the melt brushes were in contact, and with no further applied load, the material in the gap was progressively extruded out, the film becoming noticeably thinner shortly after the layers come into adhesive contact. The adhesion between the brush covered surfaces results from the interfacial free energy gain when two brush/air interfaces are replaced by a single brush/brush interface of lower energy. On approach the surfaces spontaneously jumped together, forming a well-defined flattened zone of radius a_{exp} in the range $15-25\ \mu$m. As soon as the surfaces jumped to adhesive contact, the bilayer film started to thin spontaneously. The gradual change with time in the position of a given fringe in contact is shown in Figure 4A. Even (as opposed to odd) fringes, which are more sensitive to the differences in the refractive indices of the medium (air) and the polymer film at the surface separations of our experiments, exhibit a characteristic "neck" which thickens with time, as shown in Figure 4B. The right of Figure 4B shows a cartoon corresponding to the geometry of the melt brushes in contact.

The size and the shape of the contact zone immediately after the jump-in, manifesting a large flattened region of the mica surfaces at the point of closest

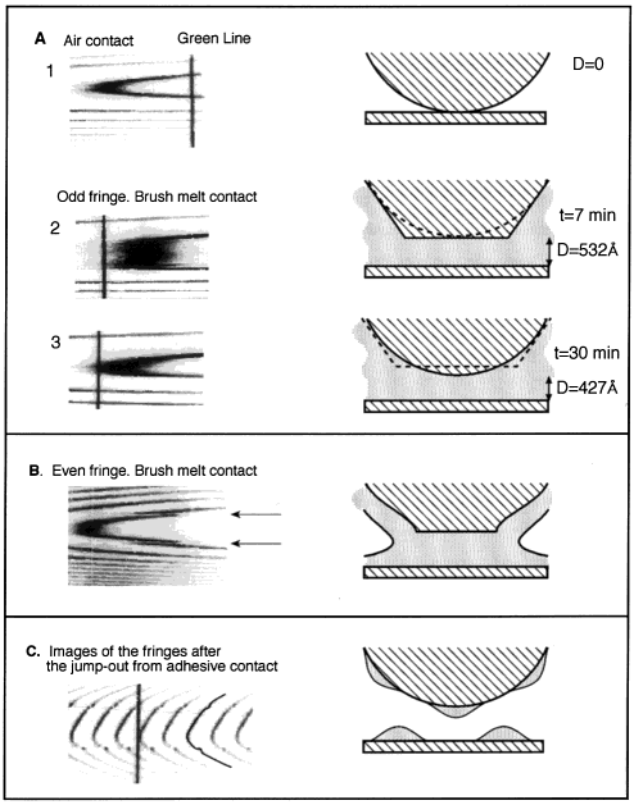

Figure 4. Video images of the ECO fringes at different stages of the experiment and sketches of the corresponding contact geometry. (A) Image 1 is the contact calibration in the air. The vertical line is a reference Hg green line. Following deposition of the PI-X layer and jump into contact, the gradual shift in the position of the *p*th-fringe (odd-order fringe) while the brush melt bilayer is thinning is illustrated in images 2 and 3, taken at a given point at the indicated times and corresponding film thickness. Sketch 3 illustrates the extruding out of the bilayer as the mica sheets "pop out" at the point of closest approach. (B) Image of an even fringe with a characteristic "neck". Even fringes are more sensitive to the differences in the refractive indexes of the medium (air) and the polymer film, so that the video image clearly shows the discontinuities (arrows) in the fringe shape corresponding to the neck. (C) Images of the fringes after the jump out, the kinks in the fringes, and their shape indicating the damage to the continuity of the polymer film (one of the fringes is highlighted to show the kinks more clearly).

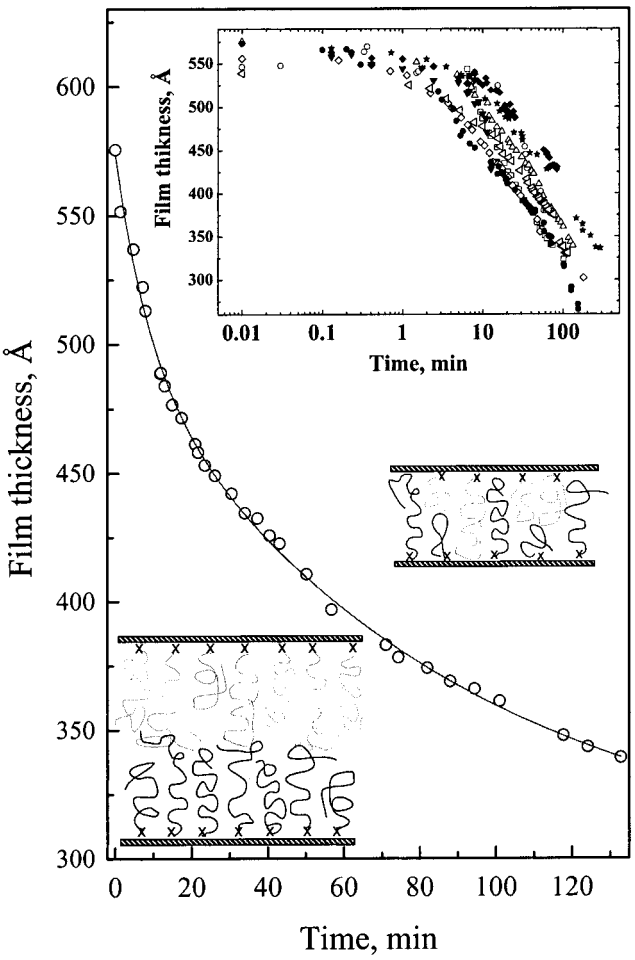

Figure 5. Kinetics of thinning of the brush melt bilayer following the jump into adhesive contact (the solid line is a double-exponential decay with two well-separated relaxation times, centered on 8 and on 116 s, applying for the first 20 min or so and for longer times). Upper inset: kinetics of the film thinning for different contact positions and experiments plotted in logarithmic scale. The cartoons illustrate the molecular structure of the brush bilayer following the jump in (bottom) and following substantial thinning, indicating the lower chain-anchoring density following the extrusion.

approach (Figure 4A(2)), are in reasonable agreement with JKR theory.[35] Thus, in the absence of an applied normal load, JKR theory relates the radius a of the contact zone to the undeformed radius of curvature R (= ca. 1 cm) of the mica surfaces as

$$a^3 = 12\pi\gamma_{PI}R^2/K \qquad (3)$$

where K is the effective bulk modulus of the PI-X melt/mica/glue/glass combination and has a value in the range[33,39] $K \approx (1-5) \times 10^9$ N/m^2, while γ_{PI} is the surface energy of the PI melt brush. Putting $\gamma_{PI} \approx 30$ mJ/m^2 and $R = 10^{-2}$ m gives $a \approx 30-50$ μm, larger but comparable with our observations ($a_{exp} = 15-25$ μm). The 2-fold variance in the measured diameter of the flat contact zone may be due to differences in the local thickness of the glue layer used to mount the mica sheet to the cylindrical glass lens or to local variations in the effective radius of curvature R. The value $R = 1$ cm used in the estimate could vary significantly in practice due to thickness variations in the glue, while very thin glue layers would result in a larger effective modulus for the PI-X melt/mica/glue/glass combination and consequently a smaller value for the contact zone radius a.

With time, not only does the film thickness at the point of closest approach decrease, but also the size and the shape of the contact zone change (as observed from the shape of the fringes). The latter effect, where the flat mica area decreases with time as the separation of closest approach decreases, is due we believe to the lateral migration of brush chains away from the middle of the contact region, where as predicted by the JKR model the highest pressure is acting. This is considered in more detail below, but qualitatively we remark that the extrusion of polymer away from the mid-contact region enables the flat mica zone to "pop out" and become more curved again, as seen in the fringe in Figure 4A(3) and indicated in the accompanying schematic figure.

Figure 5 shows the thinning of the polymer bilayer as a function of time following their spontaneous jump into contact. Such kinetic curves of the film thinning are quite reproducible from different experiments (dif-

ferent pairs of mica sheets) and different contact positions within experiments (upper inset to Figure 5). The upper inset to Figure 5 indicates that within the first minute or so after the jump-in the film thickness decreases by about 25 ± 5 Å. Within the first 10−20 min after the surfaces have been in contact the brush bilayer loses about 20% of its initial thickness, following which the flow of the brush melts becomes more sluggish, with thinning velocity reduced to about 1 Å/min. Over a period of 2−3 h the film thickness decreases to about 300 Å. The kinetic data over this period may be fitted by a double-exponential decay for the initial and later periods of thinning, as is shown by the solid curve in the main figure. The mechanism of this thinning is considered later.

We emphasize that throughout the experiments external load was never applied to the surfaces following their jump into contact. However, even in the absence of such a load, JKR theory tells us that under adhesive forces two contacting bodies experience a "contact-induced" normal stress, with a compressive maximum in the center of the contact zone, decreasing to negative (tensile) values toward the edges (see later discussion, especially Figure 9A). We note here that the compressive pressure at the center of the contact zone may be estimated from the JKR theory[35] for our system (see eq 4 later) to be of order 10 MPa (100 atm) even without any external applied load.

Qualitatively, we attribute the thinning of the brush melt to the lateral pressure gradient arising from the normal stress, which must cause the zwitterion groups anchoring the chains to the mica to migrate laterally away from the contact-zone midpoint (where the pressure is highest). The chains are then partially squeezed out toward the edges of the contact, thus decreasing the surface coverage. This issue is considered more quantitatively later. We note that in our system a residual interfacial layer of water may remain on mica surface after the deposition of the polymer film from the water subphase, which could facilitate the lateral sliding of the zwitterion groups.

Adhesion Measurements. The use of the JKR expression (eq 1) to evaluate surface energies is complicated when the surfaces are viscoelastic,[40] as in the case of polymer surface layers above their T_g as in the present study, due to pull-off rate dependence of F_p. Recent SFB studies on the pull-off forces of thin layers (ca. 1−3 nm) of PVP−polyisoprene[21] and on the similar PVP−polybutadiene[22] block copolymers have been carried out to probe the viscoelastic adhesion mechanism in these polymer melt films. The values obtained for the surface energies in those studies were substantially larger than literature values, an effect attributed to the larger magnitudes of F_p resulting from finite pull-off rates[22] or to the opportunity for the highly flattened tethered chains to expand 2-fold on being brought into contact with a similar layer, which leads to a more favorable contact energy.[21] We observed some similarities to this in the behavior of the PI-X brush melt on separation from adhesive contact, as well as some different features, and we summarize our findings below.

On separation from the flattened contact between PI-X brush monolayers the contact area gradually decreases and finally appears as a point just before the jump out occurs. Such pointlike behavior prior to separation is not predicted by the JKR model which

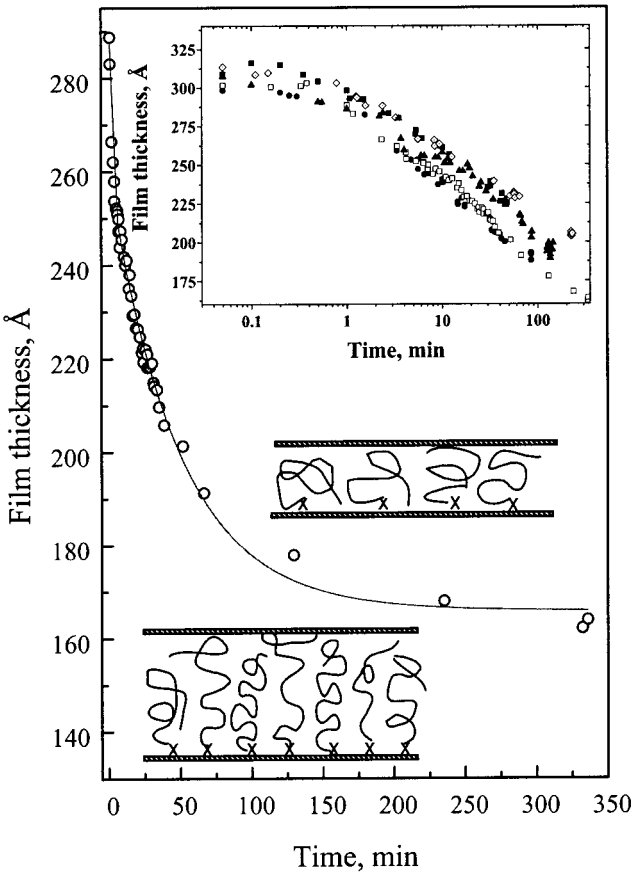

Figure 6. Kinetics of thinning of the brush melt monolayer following the jump into adhesive contact (the solid line is a double-exponential decay with two well-separated relaxation times, centered on ca. 3 and on 65 s, applying for the first 10 min or so and for longer times). Upper inset: kinetics of the brush monolayer thinning measured during the aging of the film up to 25 days. The data shown were taken following 1 day (triangles), 2 days (open diamonds), 5 days (open squares), 9 days (filled circles), and 25 days (filled squares) after deposition. The cartoons illustrate the molecular structure of the brush monolayer following the jump in (bottom) and following substantial thinning, indicating the lower chain-anchoring density following the extrusion.

deals with purely elastic surfaces. This point deformation is very pronounced (pointlike contacts prior to pull-off have been noted earlier[22]) and is accompanied by slow expansion of the film after the decompression load was applied; the surface separation just before pull-off from the point contact is shifted outward by up to 50−70 Å in a manner, suggesting the formation of a thin neck (due to interpentration of the opposing layers and their subsequent sticking together on separation) right before the jump apart. The changes in the shear response of the film while receding will be described separately.[25] The formation of such a point deformation on receding may be due to the nonuniform stress distribution within the contact zone (Figure 6), which leads to a higher degree of interdiffusion and entanglements, and hence of adhesive energy toward the center of the contact zone.

In contrast to previous studies,[21,22] which have shown an increase of over 50% in the surface energies determined from the pull-off values compared with their thermodynamic values, we did not measure a similar enhancement in our investigation. The origin of the anomalously higher values in these earlier studies is believed to be an effectively enhanced adhesion resulting

from viscoelastic effects at the finite pull-off rates between the mutually interpenetrated polymer−melt layers on the opposing surfaces. In our experiments the surface energy of each brush layer, determined from the pull-off force via eq 1, was in the range $\gamma_{PI} = 33 \pm 5$ mN/m, closely similar to the literature value[32] for bulk polyisoprene, which is in the range 30−34 mN/m.. The apparent absence of any viscoelastic enhancement of the pull-off forces in our study, despite the high degree of interpenetration expected for the PI-X brush melts, can be understood by the damage to the brush structure on separation. We observed that each time, following the jump out, the ECO fringes (which map the relative contact geometry) appeared to show intermittent discontinuities (Figure 4C). This indicates that the layers are no longer uniform following the jump-out (as otherwise the fringes would be smooth and continuous). This is likely due to some detaching of the end groups from the mica surface, resulting in a partially peeled film as indicated schematically in Figure 4C. A simple estimate supports this picture: if we assume that the adhesive energy $\gamma_{PI/mica}$ between each brush layer and the underlying substrate is due mainly to the zwitterion/mica interaction, we may estimate $\gamma_{PI/mica} = (\epsilon_{zwitterion/mica}/A) \cong 20$ mJ/m^2, where we use the previously determined[6] values $\epsilon_{zwitterion/mica} = 8k_BT$ and $A = 170$ Å^2. (We note that the value of $\epsilon_{zwitterion/mica}$ obtained from ref 6 is with respect to toluene rather than to other PI segments as in the present study.) Thus, $\gamma_{PI/mica}$ is substantially lower than γ_{PI}, and on pulling apart the weakest plane, where separation therefore occurs, is at the polymer/mica rather than the polymer/polymer interface, avoiding the regions of highly interpenetrated and entangled chains from the opposing layers. For this reason we measure a pull-off force which is less than might have been expected if viscoelstic enhancement effects at the interpenetrated brush−brush interface had been dominant (the fact that our measured value is actually close to the thermodynamic literature value for γ_{PI} is fortuitous).

Single PI-X Brush Trapped between Mica Surfaces. We examined the behavior when a brush layer was deposited only on one of the mica surfaces and the other remaining bare. In this case too a jump-in was observed on approach, with flattening of the contact zone and a spontaneous thinning with time of the brush monolayer (Figure 6). The surface separation following the jump-in was 305 ± 6 Å, close to the brush thickness $h = 302 \pm 10$ Å calculated from eq 2 and to half the jump-in separation when both surfaces were covered with a brush. The thinning behavior (i.e., dD/dt) with time shown in Figure 6 resembled that of the brush bilayer, save that it was more sluggish, with a thickness decrease of ca. 15 ± 5 Å in the first minute, about half the thinning rate of the bilayer. A double-exponential fit could again describe the data over the time of measurements (solid curve through the data in Figure 6). We note also that the radius of the flattened contact area for the monolayer just after the jump-in was generally smaller than for the bilayer case, with $a_{exp} = 10-15$ μm, roughly $^2/_3$ its value for the two brush case. With reference to eq 3, this decrease is likely to be to a combination of a somewhat lower value for the interfacial energy, together with a possibly larger value for the effective modulus K, since the thickness of the more compressible polymer melt layer is smaller in the case of the monolayer.

In general, a given experiment was completed within some days. However, measurements carried out on one of our monolayer samples at several contact positions over a 25 day period, while the SFB was kept in a clean air environment and shortly exposed to white light for measurements, provide revealing information on the PI-X brush stability with respect both to dewetting from the mica surface and to cross-linking within the brush layer itself. As seen in the inset to Figure 6, the initial thickness of the film at these different positions, as well as the kinetic monolayer thinning data taken at different times, are within the normal scatter between different contact positions. Moreover, the uniform (continuous) nature of the fringes on consecutive approach runs and in contact also confirmed that the PI-X film retained its integrity throughout.[41] Another indication that the PI-X films retains their integrity and remain un-cross-linked with time was obtained from equilibrating the brush melt in a good solvent (cyclohexane). We found that chains swell and then desorb from the surface leaving a certain equilibrium surface coverage. Interestingly, this surface coverage was similar to the equilibrium adsorption obtained by self-assembling of PI-X chains from the polymer solution in cyclohexane. These data will be reported on separately but are mentioned here as support for the present results.

AFM scans of the PI-X monolayers deposited on freshly cleaved mica sheets did not reveal any signs of dewetting or inhomogeneous domains even following 6 months of aging in a clean dry atmosphere and showed surface roughness of only some 5 Å (Figure 7).

Refractive Index Measurements. The motivation for measuring the refractive index of the PI-X brush films was to obtain if possible insight into the stretched structure of the brush melt. It is known that orientation or phase changes may contribute to variations in the index of refraction of a polymer with a given chemical structure.[32]

Refractive index profiles $n(D)$ of the PI-X monolayers (Figure 8a) and bilayers (Figure 8b) were measured during the thinning of the films in the range of 550−190 Å. Both the mean value 1.52 ± 0.01 measured for the bilayer and that of 1.51 ± 0.01 measured for the monolayer are, within the scatter, identical to the refractive index of bulk polyisoprenes,[32] $n_D = 1.521$. This shows that the optical properties within the brush melts are similar to the bulk, and that any deviation due to chain stretching is smaller than our resolution.

Brush Interpenetration and Mechanism of Contact Thinning. It is unfortunately not possible to measure directly the extent of brush−brush interpenetration from the SFB experiments on the brush melts (or on solvated brushes). This is because the separations measured when the brush layers are in contact depend only on the total amount of polymer between the surfaces, not on its conformation or extent of interpenetration. When we come to consider the shear forces between brushes,[25] however, the extent of interpenetration will play an important role, and comparison of models with the measured shear forces will provide insight into this.

We come finally to consider the process leading to the thinning of the brush layers when in adhesive contact. Qualitatively, as noted earlier, this occurs because the chains are squeezed out of the contact zone by the adhesion-induced contact pressure. The energy associated with *sliding* of the zwitterion groups along the mica

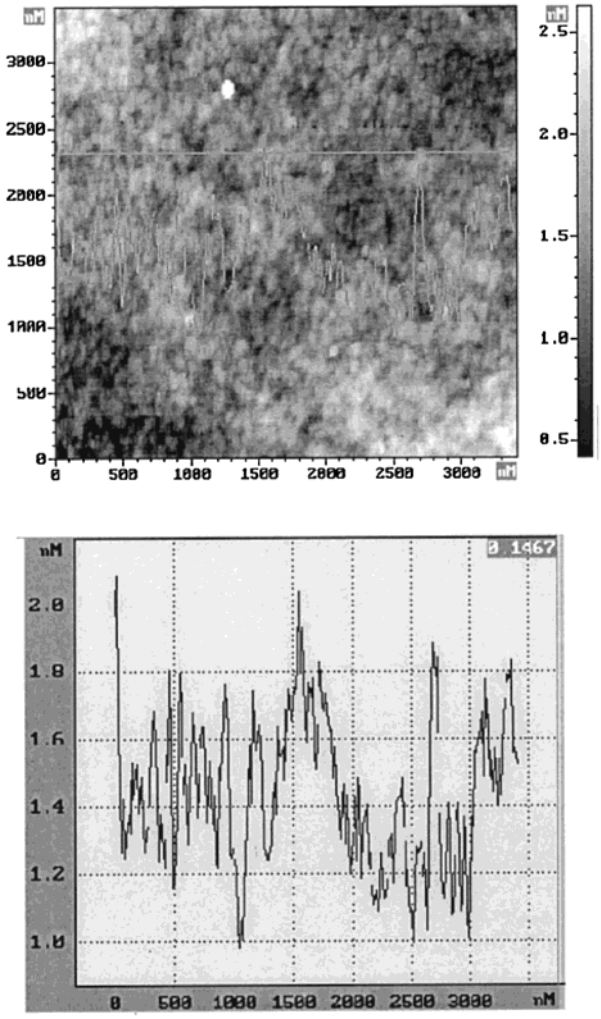

Figure 7. AFM image of the PI-X brush melt aged for 6 months. The image shows a homogeneous film with a surface roughness of ca. 5 Å.

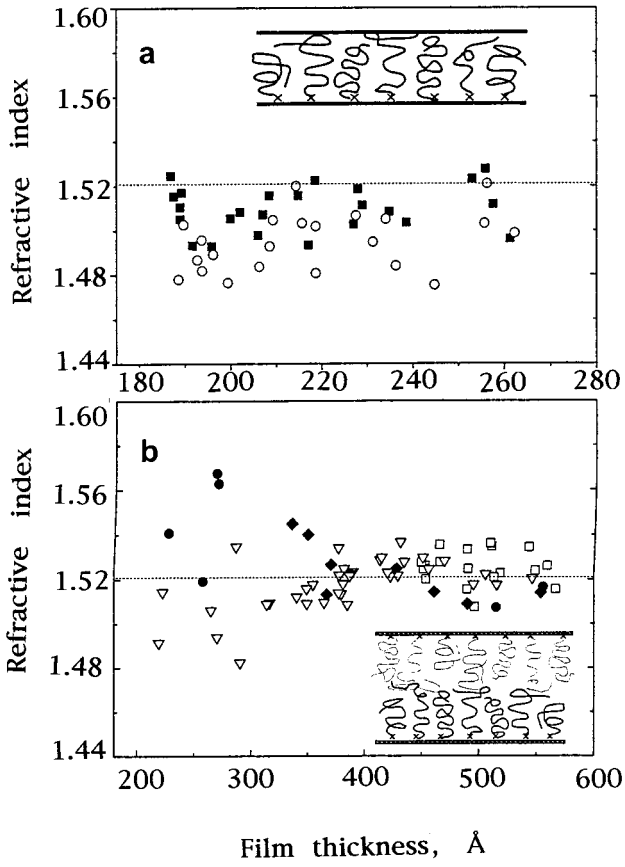

Figure 8. Variation of the refractive index as a function of the film thickness. Different symbols correspond to different experiments. (a) For the monolayer the averaged refractive index is 1.51 ± 0.01. (b) The averaged value for the bilayer is 1.52 ± 0.01. In both cases the measured values are very close to the refractive index of the bulk polyisoprenes $n_D = 1.521$, shown as dashed line. Data points are based on the mean of several readings of each fringe-tip position, which considerably reduces the scatter.

surfaces, as opposed to their total detachment considered earlier, may be quite low; this is especially the case when one considers that during the LB deposition process a thin residual water layer is likely to remain at the mica/polymer interface. The adhesion-induced pressure within the melt brushes thus readily results in lateral motion of the anchoring chain ends, and the kinetically limiting step is the viscous resistance of the brush bilayer (or monolayer) to being squeezed out. In what follows we explore this mechanism more quantitatively.

To facilitate further discussion, we show in Figure 9 schematically the confined brush melt film (A) just after the jump into contact, (B) a short while later, and (C) at a much later stage (compare with Figure 4C). Just after the jump-in (Figure 9A), the brush bilayer is confined within a thin disk of radius a, within which the pressure distribution $\sigma(r)$ is as shown. From the JKR model[35,39] we have the form of the distribution

$$\sigma(x) = \frac{3Ka}{2\pi R}(1 - x^2)^{1/2} - \left(\frac{6K\gamma_{PI}}{2\pi a}\right)^{1/2}(1 - x^2)^{-1/2} \quad (4)$$

where $x = r/a$. The total effective adhesion-induced force F_{eff} on the disk, given by integrating the stress over the total disk area, is—in the absence of any applied normal load—simply zero. However, within the region where the normal stress $\sigma(r) > 0$, limited by the radius $r_0 = ax_0$, there will be a net compressive force, and it is from within this region that the brush melt will be squeezed out. To find r_0, we equate the right-hand side of eq 4 to zero, giving $x_0 = r_0/a = (2/3)^{1/2}$; i.e., the squeeze-out region has a radius r_0 which is over 80% of the full radius a of the flattened disk. Although the pressure distribution has a maximum in the center ($r = 0$) and is highly nonuniform, we may nonetheless proceed to evaluate the total compressive force F_0, by integrating the stress across the area of the disk of radius r_0:

$$F_0 = \int_{r=0}^{r=r_0} 2\pi r\sigma(r)\, dr = a^2 \int_{x=0}^{x=x_0} 2\pi x\sigma(x)\, dx \quad (5)$$

Substituting for $\sigma(x)$ from eq 4 and making use of the relation $a^3 = 12\pi\gamma_{PI}R^2/K$ from eq 3, we find after some algebra that $F_0 = C\gamma_{PI}R$, where the value of the constant is given by

$$C = 12\{[1 - (1/3)^{3/2}] - [1 - (1/3)^{1/2}]\} \approx 4.6$$

It is of interest that this compressive force $F_0 \approx (F_{pulloff}/2)$, where $F_{pulloff} = 3\pi\gamma_{PI}R$ is the force required to pull the adhered bilayers apart.

We now assume that we may apply the hydrodynamic equation, originally due to Reynolds,[42] relating the approach rate (dD/dt) of a disk of radius r_0 parallel to a

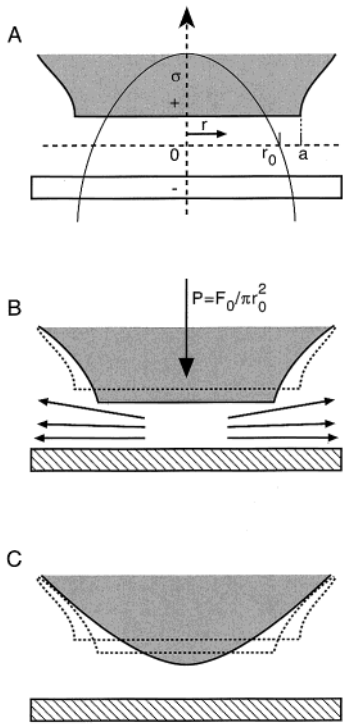

Figure 9. Illustrating our model for the extrusion of the melt brush layers following their jump into contact. (A) Just after jump-in. The form of the stress distributions $\sigma(r)$ (shown by the solid curve, where "+" indicates compressive and "−" indicates a tensile stress) is given by eq 4, where a is the contact radius and r_0 is the radius over which the normal stress is compressive. (B) Over the initial period following the jump-in the extrusion may be viewed as resulting from the pressure P on a disk of radius roughly r_0, where P is the mean pressure due to the total compressive force F_0 over the area πr_0^2. The broken silhouette is the contact zone shape corresponding to A. (C) At longer times the flattened contact area "pops out" under the pressure maximum at the point of closest approach, as suggested by fringe-shapes as in Figure 4A(3). The broken silhouettes are the contact zone shapes corresponding to (A) and (B).

flat surface a distance D away ($D \ll r_0$), when compressed at pressure P across a liquid of viscosity η:

$$\mathrm{d}D/\mathrm{d}t = -2D^3P/(3\eta r_0^2) \qquad (6)$$

In order for this to be valid for the compression of the melt brushes within the disk of radius r_0 (Figure 9A), we have to assume that the pressure is uniformly distributed (which is a simplification in view of the maximum in the center of the contact disk) and furthermore to ignore the tensile region at $r > r_0$. If we do this and take $P = F_0/(\pi r_0^2)$, we obtain

$$\mathrm{d}D/\mathrm{d}t = -2D^3F_0/(3\eta\pi r_0^4) \qquad (7)$$

This relation is likely to be most valid just following the jump into contact, as subsequently the central region of the contact disk curves out (as indicated by the shape of the fringes, Figure 4A3, and shown schematically in Figure 9C), and the compressive stress is greatly reduced. We may at this level of approximation take the viscosity of the confined brush melt to be that of bulk PI (of corresponding molecular weight). To compare with experiment, we put in values for the various parameters for the bilayer case: D = 560 Å, η = 230 Pa·s, $F_0 = C\gamma_{PI}R$, with γ_{PI} = 30 mJ/m^2 and R = 1 cm, and $r_0 = (2/3)^{1/2}a$ where we take a = 50 μm in line with our estimates from eq 3. Using these values, we find for the brush bilayer just after the jump into contact that $\mathrm{d}D/\mathrm{d}t = -0.35$ Å/s $\approx$ 20 Å/min. This is close to or slightly less than the observed thinning rate of ca. 25 ± 5 Å/min in the first minute or so after the jump-in (inset to Figure 5).

We note a number of simplifications in our treatment: the hydrodynamic relation in eq 6 assumes that the pressure P is uniform across the disk, while in practice the normal stress $\sigma(r)$ has a maximum at the disk center, and we have also ignored the effect of the tensile stress (which would act to reduce the squeeze-out force). In addition, the result in eq 6 assumes a Poisseuille-like velocity profile of the extruded liquid, whereas in practice, since all polymer molecules in the gap are in contact with one surface or another (via the sliding zwitterion groups) as they are squeezed out, the flow must have a plug-like profile. This would increase the effective viscosity and result in a lower predicted thinning rate. Finally, we use a value for the radius of contact a based on eq 3, while the experimental value a_{exp} is roughly half of that, which would result in a larger predicted thinning rate. These different simplifications act in opposing directions, and overall we feel that our predicted thinning rate is likely to be a good estimate for the actual experiments. The quantitative agreement of the predicted with the observed initial thinning rate, even if perhaps fortuitously close, is thus a good indication that our model for the extrusion is realistic.

An interesting internal check on this validity is provided by applying our model to the extrusion of the melt brush *monolayer*. Since the magnitude of D in this case just after the jump-in is roughly half of its value for the bilayer, then from eq 7, which has a D^3 dependence, we would expect the thinning rate to be reduced to $^1/_8$ of the bilayer value. However, account must also be taken of the smaller value of the flattened contact radius for the brush monolayer case, which is observed to be 10−15 μm, or some $^2/_3$ of the bilayer value. The r_0^{-4} dependence in eq 7 then restores the magnitude of the predicted thinning rate ($\mathrm{d}D/\mathrm{d}t$) for the monolayer to be ca. 0.6 of its value for the bilayer, closely in line with what is observed (compare the experimentally measured thinning rates of 15 Å/min for the monolayer vs 25 Å/min for the bilayer, immediately following the jump-in to contact in the two cases).

Our picture of the thinning process is thus as follows: just after the jump into contact, the adhesion-induced pressure results in extrusion of the confined brushes (bilayer or monolayer), via sliding of the anchoring zwitterion groups along the mica surfaces. The thinning of the layers can be quantitatively described using a simplified treatment based on the JKR model together with a Reynolds-like equation relating the extrusion of liquid between a disk compressed onto a flat. This treatment is most valid during the initial stages, following which the flattened mica surfaces "bow out" and become curved again as polymer is squeezed out (Figure 9C). This reduces the elastic compressive energy and, together with the thinner layers, results in progressively slower thinning of the confined brushes, as indeed observed.

Summary. Dense PI-X melt brush layers (an order of magnitude denser than previous studies of confined melt brushes) were created on mica via LB deposition.

Their integrity, thickness, and behavior on confinement once they had come into adhesive contact were determined using an SFB, as a preliminary to shear measurements, both for bilayers (a brush on each interacting mica surface) and for a monolayer (a single brush layer facing a bare mica surface). Once the layers had jumped into adhesive contact, progressive thinning of the confined melt brushes occurred, slowing down from an initially rapid rate, until—over the time scale of our measurements, some hours—extrusion of the confined brushes down to some (0.5−0.7) of their initial thickness had occurred. Refractive index profiles during the thinning process revealed no deviation of the refractive index—within the scatter of our measurements—from its bulk value, suggesting that within these limits any effects resulting from chain extension were below our resolution. A model for the chain extrusion, based on the idea that compressive elastic energy due to the adhesion was driving the chains to move laterally via the sliding of the zwitterionic anchoring groups on the surfaces, was in fair quantitative agreement with our observations. In paper 2 of this series we examine the shear forces between the PI-X melt brushes when they are made to slide past each other.

Acknowledgment. We thank Pavel Protsenko for assistance in assembling the LB device and help with preparation of the manuscript. We are grateful to the Deutsches-Israelische Program (DIP), the US−Israel Binational Science Foundation, and the Minerva Foundation for their support of this work.

References and Notes

(1) For a recent review, see: Grest, G. S. Normal and shear forces between polymer brushes. *Adv. Polym. Sci.* **1999**, *138*, 149.
(2) Dolan, A. K.; Edwards, S. F. *Proc. R. Soc. London* **1975**, *A343*, 427.
(3) Alexander, S. *J. Phys. (Paris)* **1977**, *38*, 983.
(4) Hadzioannou, G.; Patel, S.; Granick, S.; Tirrell, M. *J. Am. Chem. Soc.* **1986**, *108*, 2869.
(5) deGennes, P. G. *Adv. Colloid Interface Sci.* **1987**, *27*, 189.
(6) Taunton, H. J.; Toprakcioglu, C.; Fetters, L. J.; Klein, J. *Macromolecules* **1990**, *23*, 571.
(7) Halperin, A.; Tirrell, M.; Lodge, T. *Adv. Polym. Sci.* **1991**, *100*, 31.
(8) Milner, S. T. *Science* **1991**, *251*, 905.
(9) Neelov, I. M.; Borisov, O. V.; Binder, K. *J. Chem. Phys.* **1998**, *108*, 6973.
(10) Napper, D. H. *Steric Stabilization of Colloidal Dispersions*; Academic: London, 1983.
(11) Fleer, G. J.; Cohen-Stuart, M. A.; Scheutjens, J. M. H. M.; Cosgrove, T.; Vincent, B. *Polymers at Interfaces*; Chapman and Hall: London, 1993.
(12) Yerushalmi-Rozen, R.; Klein, J.; Fetters, L. J. *Science* **1994**, *263*, 793.
(13) Klein, J.; Kumacheva, E.; Mahalu, D.; Perahia, D.; Fetters, L. J. *Nature (London)* **1994**, *370*, 634.
(14) Klein, J. *Annu. Rev. Mater. Sci.* **1996**, *26*, 581.
(15) Witten, T. A.; Leibler, L.; Pincus, P. A. *Macromolecules* **1990**, *23*, 824.
(16) Joanny, J. F. *Langmuir* **1992**, *8*, 989.
(17) Nemirovsky, A. M.; Witten, T. A. In *Stress Relaxation in Diblocks*; Garrido, L., Ed.; Springer-Verlag: Heidelberg; 1993.
(18) Van Alsten, J.; Granick, S. *Macromolecules* **1990**, *23*, 4856.
(19) Hirz, S.; Subbotin, A.; Frank, C.; Hadziioannou, G. *Macromolecules* **1996**, *29*, 3970.
(20) Luengo, G.; Schmitt, F.; Hill, R.; Israelachvili, J. *Macromolecules* **1997**, *30*, 2482.
(21) Watanabe, H.; Tirrell, M. *Macromolecules* **1993**, *26*, 6455.
(22) Ruths, M.; Granick, S. *Langmuir* **1998**, *14*, 1804.
(23) Ruths, M.; Johannsmann, D.; Ruhe, J.; Knoll, W. *Macromolecules* **2000**, *33*, 3860.
(24) Heger, R.; Goedel, W. A. *Macromolecules* **1996**, *29*, 8912.
(25) Tsarkova, L. A.; Zhang, X.; Klein, J.; Hadjichrisitidis, N. *Macromolecules*, in press.
(26) Pispas, S.; Pitsikalis, M.; Hadjichristidis, N.; Dardani, P.; Morandi, E. *Polymer* **1995**, *36*, 3005.
(27) Young, R. N.; Quirk, R. P.; Fetters, L. J. *Adv. Polym. Sci.* **1984**, *56*, 1.
(28) Widmaier, J. M.; Meyer, G. C. *Macromolecules* **1981**, *14*, 450.
(29) Davidson, N. S.; Fetters, L. J.; Funk, W. G.; Graessley, W. W.; Hadjichristidis, N. *Macromolecules* **1988**, *21*, 112.
(30) Hadjichristidis, N.; Zhongde, X.; Fetters, L. J. *J. Polym. Sci., Polym. Phys. Ed.* **1982**, *20*, 743.
(31) Pearson, D. S.; Mueller, S. J.; Fetters, L. J.; Hadjichristidis, N. *J. Polym. Sci., Polym. Phys. Ed.* **1983**, *21*, 2287.
(32) Brandrup, J.; Immergut, E. H.; Grulke, E. A. *Polymer Handbook*, 4th ed.; J. Wiley & Sons: New York, 1999.
(33) Klein, J.; Kumacheva, E. *J. Chem. Phys.* **1998**, *108*, 6996.
(34) Israelachvili, J. N. *J. Colloid Interface Sci.* **1973**, *44*, 259.
(35) Johnson, K. L.; Kendall, K.; Roberts, A. D. *Proc. R. Soc. London* **1971**, *A324*, 301.
(36) Kekicheff, P.; Spalla, O. *Langmuir* **1994**, *10*, 1584.
(37) Fytas, G.; Anastasiadis, S. H.; Seghrouchni, R.; Vlassopoulos, D.; Li, J.; Factor, B. J.; Theobald, W.; Toprakcioglu, C. *Science* **1996**, *274*, 2041.
(38) deGennes, P.-G. *Scaling Concepts in Polymer Physics*; Cornell University Press: Ithaca, NY, 1979.
(39) Chen, Y. L.; Helm, C. A.; Israelachvili, J. N. *Langmuir* **1991**, *7*, 2694.
(40) Mangipudi, V. S.; Tirrell, M. *Rubber Chem. Technol.* **1998**, *71*, 407.
(41) Interestingly, this contrasts with the properties of shorter PI brushes (M = 11.9K, kindly donated by W. Goedel, to be published), end-terminated with sulfonate groups rather than with sulfozwitterionic groups as in our samples, where both the shape of the fringes and AFM measurements clearly indicated dewetting of the brush melt from mica already within several days. This suggests that mica is intrinsically dewetted by PI (though the detailed PI microstructure may play a role) and that our melt brush layers were kinetically rather than thermodynamically stable (for possible origins of this, see: Safran, S. A.; Klein, J. *J. Phys. II* **1993**, *3*, 749−757).
(42) Reynolds, O. *Philos. Trans. R. Soc. London* **1886**, *177*, 157.

MA010981F